Journal of Applied Physics

High thermoelectric figure of merit in monolayer Tl_2O from first principles

Cite as: J. Appl. Phys. **128**, 185111 (2020); https://doi.org/10.1063/5.0030588
Submitted: 23 September 2020 . Accepted: 02 November 2020 . Published Online: 12 November 2020

Qingjun Huang, Jinlong Ma, Dongwei Xu, Run Hu, and Xiaobing Luo

Journal of Applied Physics ARTICLE scitation.org/journal/jap

High thermoelectric figure of merit in monolayer Tl_2O from first principles

Cite as: J. Appl. Phys. **128**, 185111 (2020); doi: 10.1063/5.0030588
Submitted: 23 September 2020 · Accepted: 2 November 2020 ·
Published Online: 12 November 2020

View Online Export Citation CrossMark

Qingjun Huang,[1] Jinlong Ma,[2,a)] Dongwei Xu,[2] Run Hu,[2] and Xiaobing Luo[2]

AFFILIATIONS

[1]State Key Laboratory of Disaster Prevention & Reduction for Power Grid Transmission and Distribution Equipment, State Grid Hunan Electric Power Corporation Disaster Prevention & Reduction Center, Changsha 410007, China
[2]School of Energy and Power Engineering, Huazhong University of Science and Technology, Wuhan 430074, China

[a)]**Author to whom correspondence should be addressed:** majinlong@hust.edu.cn

ABSTRACT

The thermoelectric properties of monolayer Tl_2O are studied using first-principles calculations with all involved electrical and thermal transport properties calculated in the parameter-free frameworks. It is found that monolayer Tl_2O possesses remarkably high thermoelectric figure of merit, zT, due to its ultralow lattice thermal conductivity and fairly good power factor. The room temperature zT can be as high as 1.4 and 1.2 for n- and p-type systems, respectively, whereas the maximum zT values can reach up to 5.3 and 4.2 as the temperature increases to 800 K. In addition, it is clarified that the mobilities of monolayer Tl_2O are orders of magnitude smaller than previous estimation from simplified semiempirical models. The room temperature electron and hole mobilities are only about 56 and 11 $cm^2 V^{-1} s^{-1}$, respectively, due to the heavy effective mass along with strong polar optical phonons coupling scattering. Nonetheless, the intrinsically ultrahigh zT from entire first-principles calculations stimulate that the further experimental verification and exploration for practical application are worthwhile.

I. INTRODUCTION

In the contradiction between the rapid increase of energy consumption and the limited resource of fossil fuels, energy recovery and reuse are the eternal themes of sustainable development. Nowadays, the energy we use is mostly generated by the thermal processes, and the energy we waste is ultimately in the form of heat. Thermoelectrics is a simple and green technology enabling direct heat-to-electricity conversion and could play an active role in the global energy solutions. The large-scale application of thermoelectrics hopes for high-energy conservation efficiency of thermoelectric materials, which is determined by a dimensionless figure of merit, $zT = \alpha^2\sigma T/(\kappa_e + \kappa_l)$,[1,2] where α, σ, κ_e, κ_l, and T denote the Seebeck coefficient, electrical conductivity, electronic thermal conductivity, lattice thermal conductivity, and absolute temperature, respectively. To realize high zT value, good electrical transport properties and, simultaneously, poor thermal transport properties are desired. Nevertheless, this is not an easy thing due to the conflicting combination of α, σ, and κ_e; thus, decoupling the required traits is imperative in the optimization strategies.[3] The most straightforward way is to expect κ_l as low as possible, since it is a phonon property which is relatively independent of the electrical properties. Looking for materials with intrinsically low κ_l, usually below 1 $Wm^{-1} K^{-1}$, is an effective mainstream.[4–10]

In the past few decades, two-dimensional (2D) materials have attracted intense interest due to reduced dimensionality, which advances the breakthrough of ultrasmall and flexible devices.[11–14] Seeking 2D thermoelectric materials with high conversion efficiency is one of the most vibrant research fields.[14,15] Though a series of 2D materials have been experimentally demonstrated to possess a large power factor ($PF = \alpha^2\sigma$) comparable with the state-of-the-art bulk thermoelectric materials, their thermal conductivities are too high for good thermoelectrics.[16–18] Therefore, great efforts have been put into finding low-κ_l 2D materials[19–23] using the parameter-free first-principles calculations.[24,25]

Recently, it is reported that monolayer Tl_2O is possibly obtained by exfoliating from its experimentally known bulk counterpart[26,27] since the cleavage energy is close to those of graphite and MoS_2. The first-principles calculations indicate that the κ_l of monolayer Tl_2O is very small, below 1 $Wm^{-1} K^{-1}$, above room temperature,[28–30] except for a literature that reported much higher values.[31] The κ_l of monolayer Tl_2O is comparable with the state-of-the-art bulk thermoelectric materials like SnSe.[4,5] Meanwhile, using the semiempirical formulas,

the electrical mobility of monolayer Tl_2O is predicted to be high.[27] The low κ_l and high mobility signify good thermoelectric promise of monolayer Tl_2O by possessing high thermoelectric zT above unity at room temperature.[30,31] However, in the calculations of electrical transport properties, single parabolic band and acoustic deformation potential model are assumed to simplify the complex band structure and electron–phonon coupling. These approximations are useful in the preliminary research but would result in physically discounted results; for instance, the calculated mobilities display surprisingly large anisotropy in the basal plane,[27] which is violated to the isotropic nature of transport properties that is guaranteed by the crystal lattice symmetry. In addition, monolayer Tl_2O is a polar system; the long-range Frölich interaction between electrons and longitudinal optical (LO) phonons, which is not considered in the acoustic deformation potential model, probably plays an important role and reduces the mobility significantly.[32–34] Therefore, inspired by the high thermoelectric potential from current estimation, we are eager to know whether monolayer Tl_2O can possess high zT if the electrical transport properties are calculated without these oversimplifications. Thus, like κ_l, the parameter-free first-principles calculations of electrical transport properties considering full electron and phonon states and electron–phonon coupling interactions are needed.

The feasible first-principles calculations of α, σ, and κ_e are about 10 years later than that for κ_l,[35] which is enabled until recently[36] in the framework of the Boltzmann transport equation (BTE) with scattering limited by the electron–phonon interactions[37] obtained from the Wannier interpolation of the density functional theory (DFT) and density functional perturbation theory (DFPT) calculations.[38] This method has demonstrated good accuracy as compared with experiments in many materials.[32,33,39–44] Although the first-principles calculations are performed for defect-free systems, its ability in predicting zT has been verified by giving fairly good agreement with experiments,[45,46] and it has been used to uncover the thermoelectric potential of many bulk and 2D materials.[47–51] Herein, we compute the full thermoelectric transport properties of monolayer Tl_2O by the first-principles calculations and the parameter-free BTE. High zT is obtained in both n- and p-type systems due to the ultralow thermal conductivity. It is also found that the actual mobility of monolayer Tl_2O is orders of magnitude smaller than the values previous predicted by the phenomenological models.

II. METHODOLOGY

From the BTE for electrons, the steady-state electrical transport properties can be derived.[36,52] The electrical conductivity tensor is written as

$$\boldsymbol{\sigma} = \frac{se^2}{\Omega N_k}\sum_{n\mathbf{k}} \mathbf{v}_{n\mathbf{k}}\mathbf{F}_{n\mathbf{k}}\left(-\frac{\partial f^0_{n\mathbf{k}}}{\partial \varepsilon_{n\mathbf{k}}}\right), \tag{1}$$

where s is the spin degeneracy, e is the elementary charge, Ω is the volume of unit cell, N_k is the number of meshes of the first Brillouin zone, $n\mathbf{k}$ is the electron state with n being the band index and $\mathbf{k}$ being the wave vector, $\mathbf{v}_{n\mathbf{k}}$ is the electron velocity, $\varepsilon_{n\mathbf{k}}$ is the electron energy, and $f^0_{n\mathbf{k}}$ is the equilibrium Fermi–Dirac distribution function. $\mathbf{F}_{n\mathbf{k}}$ denotes the converged mean free displacement from the iterative solution of BTE with all quantities computed from first principles.[32,33,52] The iterative process is started from $\mathbf{F}^0_{n\mathbf{k}} = \mathbf{v}_{n\mathbf{k}}\tau_{n\mathbf{k}}$ with $\tau_{n\mathbf{k}}$ being the electron relaxation time or the inverse of scattering rate. Dividing $\boldsymbol{\sigma}$ by the carrier concentration n_c, the mobility is obtained as $\boldsymbol{\mu} = \boldsymbol{\sigma}/(en_c)$. The Seebeck coefficient and electronic thermal conductivity tensors also can be obtained as[36]

$$\boldsymbol{\alpha} = \frac{\boldsymbol{\sigma}^{-1}se}{T\Omega N_{\mathbf{k}}}\sum_{n\mathbf{k}} (\varepsilon_{n\mathbf{k}} - \varepsilon_f)\mathbf{v}_{n\mathbf{k}}\mathbf{F}_{n\mathbf{k}}\left(-\frac{\partial f^0_{n\mathbf{k}}}{\partial \varepsilon_{n\mathbf{k}}}\right) \tag{2}$$

and

$$\boldsymbol{\kappa_e} = \frac{s}{T\Omega N_{\mathbf{k}}}\sum_{n\mathbf{k}} (\varepsilon_{n\mathbf{k}} - \varepsilon_f)^2\mathbf{v}_{n\mathbf{k}}\mathbf{F}_{n\mathbf{k}}\left(-\frac{\partial f^0_{n\mathbf{k}}}{\partial \varepsilon_{n\mathbf{k}}}\right) - T\boldsymbol{\sigma}\boldsymbol{\alpha}^2, \tag{3}$$

where ε_f is the chemical potential.

Analogously, the lattice thermal conductivity tensor can be obtained by solving the BTE for phonons, as[24]

$$\boldsymbol{\kappa_l} = \frac{1}{\Omega N_q}\sum_{\mathbf{q}p} \hbar\omega_{\mathbf{q}p}\mathbf{v}_{\mathbf{q}p}\mathbf{F}_{\mathbf{q}p}\frac{\partial n^0_{\mathbf{q}p}}{\partial T}, \tag{4}$$

where $\mathbf{q}p$ is the phonon state labeled by the wave vector $\mathbf{q}$ and mode index p, N_q is the $\mathbf{q}$ points sampled in the first Brillouin zone, $\hbar$ is the reduced Planck constant, $\omega_{\mathbf{q}p}$ is the phonon frequency, $\mathbf{v}_{\mathbf{q}p}$ is the phonon group velocity, $n^0_{\mathbf{q}p}$ is the Bose–Einstein distribution function, and $\mathbf{F}_{\mathbf{q}p}$ is the phonon mean free displacement obtained by iteratively solving the phonon BTE, which is also started from $\mathbf{F}^0_{\mathbf{q}p} = \mathbf{v}_{\mathbf{q}p}\tau_{\mathbf{q}p}$ with $\tau_{\mathbf{q}p}$ being the inverse of phonon scattering rate.[24]

For computational details, the Quantum ESPRESSO package[53] was used to carry out the DFT and DFPT calculations. The full-relativistic norm-conserving pseudopotentials[54] with Perdew–Burke–Ernzerhof (PBE)[55] exchange-correlation functional and a plane wave kinetic energy cutoff of 80 Ry were employed. Monolayer Tl_2O has a hexagonal lattice structure in the basal plane belonging to the $P\bar{3}m1$ symmetry group.[26] The relaxed lattice constant is 3.60 Å, in good consistence with previous calculations[27–31] and close to the experimental value of its bulk counterpart (3.51 Å).[56] The out-of-plane lattice parameter was fixed to be 20 Å in the calculations, whereas for the properties normalized by the volume, a nominal thickness of 6.96 Å was used for the scaling, which is the distance between the two surface Tl atomic plane plus the van der Waals radii of the two surface Tl atoms. From the computational formulas, it is known that the μ, α, and zT are numerically irrelevant to volume, whereas σ, κ_e, κ_l, n_c, and PF need be scaled up.

To calculate electrical transport properties, the electronic band structure and phonon dynamical properties were initially calculated on $8 \times 8 \times 1$ $\mathbf{k}$ and $8 \times 8 \times 1$ $\mathbf{q}$ grids, respectively. Then, the EPW package[57] was used to calculate the electron–phonon coupling matrix and interpolate these intermediate quantities to dense grids based on maximally local Wannier functions. Specifically, for electrons, the $\mathbf{k}$ and $\mathbf{q}$ grids were interpolated to $160 \times 160 \times 1$, whereas the final grids for holes were $120 \times 120 \times 1$. The polar correction for phonon dispersion and electron–phonon coupling

were extended using 2D Coulomb interaction model,[58,59] which has been examined to give physically correct results.[34] The phonon transport properties were calculated using ShengBTE package[24] with $120 \times 120 \times 1$ **q** grids. The third-order interatomic force constants were obtained by the finite displacement method using a $4 \times 4 \times 1$ supercell with $2 \times 2 \times 1$ **k** grids, and a truncation distance of 0.7 nm was adopted. These computational parameters can ensure the convergence of the electrical and thermal transport calculations (cf. Secs. I and II in the supplementary material). Since the transport properties of monolayer Tl_2O in the basal plane are isotropic due to the constraint of crystal lattice symmetry, they are presented as scalars hereafter unless otherwise noted.

III. RESULTS AND DISCUSSION

Considering the heavy atomic mass of Tl, the spin orbit coupling (SOC) was included in all of the calculations. Figure 1(a) shows that the band structure of monolayer Tl_2O is slightly affected by the SOC, yielding a little smaller bandgap of 0.92 eV at M point, in consistent with previous calculations.[29] The bandgap with PBE+SOC is smaller than that calculated with HSE+SOC (1.56–1.62 eV)[27–29] and mBJ +SOC (1.52 eV).[31] Therefore, we performed the GW correction using Yambo code[60] and obtained a larger bandgap of 1.53 eV (cf. Fig. S4 in the supplementary material). Since the bandgap is more than ten times larger than the thermalization energy within the temperatures concerned in this work, i.e., $10(k_BT) \approx 0.69$ eV at 800 K, the bipolar effect is negligible;[49,61] thus, we can calculate the electron and hole transport properties separately using the conduction bands and the valence bands. As a rule, the chemical potential is manually shifted away from the conduction band minimum or valence band maximum to characterize different carrier concentrations. Therefore,

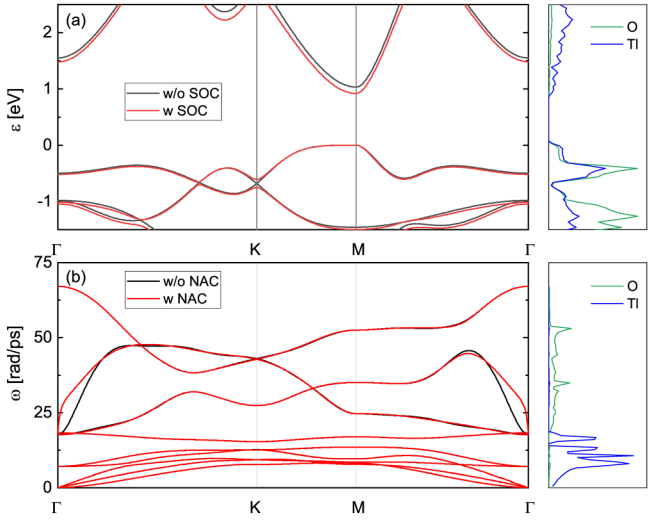

FIG. 1. (a) Electronic band structure of monolayer Tl_2O with (red) and without (black) spin orbit coupling (SOC) and the electronic projected density of states. (b) Phonon dispersion with (red) and without (black) non-analytical correction (NAC) and the phonon projected density of states.

the calculated electrical transport properties are irrelevant to the bandgap, instead, they are more related to the shape of bands. In current framework of the full first-principles calculation of electrical transport, the electron–phonon coupling cannot be calculated including the many-body correction; only the correction on the band structure can be considered.[42,44,57] We calculated the zT with the GW corrected band structure and found that the overall results have never changed substantially (cf. Fig. S5 in the supplementary material), so in order to keep the self-consistency of all involved calculations, the GW corrections are not considered in subsequent results. The electronic projected density of states was calculated. Around band edges, the conduction bands are mainly formed by the Tl atom, whereas for the valence bands the Tl and O atoms have comparable contribution. The electronic density of state around the valence band edge is larger than that around the conduction band edge, implying that the effective mass of hole is heavier than that of an electron. Actually, as the electronic bands around band edges are flat, the effective masses for electron and hole are both large, as evidenced from the fitted effective mass along some specified directions.[27,30,31]

There are three atoms in the unit cell of monolayer Tl_2O, corresponding to nine phonon branches as shown in Fig. 1(b). For the dipole–dipole interaction, the non-analytical correction in the 2D framework was employed, giving vanishing LO and transverse optical (TO) splitting at the zone center.[58] It also can be seen that the polar effect only obviously affect the highest LO phonon modes. The phonon dispersion exhibits an interesting feature that the three acoustic branches and the lowest three optical branches are particularly suppressed to flat, whereas the highest three optical branches span a wide range with steep fluctuation, which is distinguished from many other 2D materials.[26,62] This can be understood from the phonon projected density of states, which reveals that the first six low branches are dominantly contributed by the Tl atom with heavy atomic mass, whereas the last three high branches are contributed by the light O atom. As a consequence, the phonon group velocity below 18 rad/ps is much smaller than that of phonons above this frequency, as shown in the inset of Fig. 2(b), where the averaged group velocity as a function frequency[63] is plotted.

Figure 2(a) shows the κ_l of monolayer Tl_2O at different temperatures. In previous literature studies, the calculated κ_l of monolayer Tl_2O has some discrepancies; except for an obviously much high value of 2.4 $Wm^{-1}K^{-1}$,[31] most of the results are within the range from 0.17 to 0.8 $Wm^{-1}K^{-1}$ at room temperature.[28–30] The discrepancy is probably due to different pseudopotentials and computational parameters used in different calculations. Herein, we have carefully checked the convergence for several important parameters affecting κ_l and ensured the calculations convincingly converged (cf. Sec. I in the supplementary material). The obtained room temperature κ_l is 0.38 $Wm^{-1}K^{-1}$. As temperature increases, κ_l decrease monotonically to 0.15 $Wm^{-1}K^{-1}$ at 800 K. In terms of overall distribution, loosely speaking, the scattering rates above 18 rad/ps are larger than that below this frequency, as shown in Fig. 2(b). Nonetheless, due to the compensation from the relatively high group velocity, the contribution from high-frequency phonons is considerable. The normalized cumulative contribution with respect to the frequency, in the inset of Fig. 2(a), indicates that more than 40% of κ_l is contributed by phonons with frequencies larger than 18 rad/ps in the temperature range of 300–800 K.

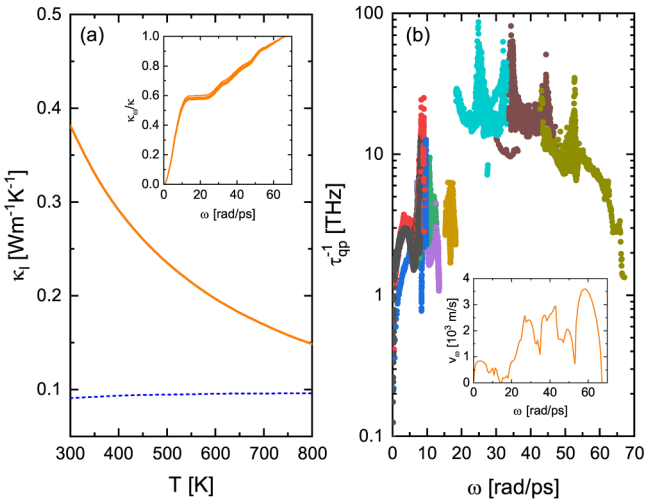

FIG. 2. (a) Lattice thermal conductivity of monolayer Tl_2O at different temperatures, with the inset being the normalized cumulative contribution from different frequencies in the temperature range of 300–800 K. The dashed line denotes the amorphous limit calculated with the Agne model. (b) Scattering rates of different phonon modes at room temperature, where the inset shows the averaged phonon group velocity at each frequencies.

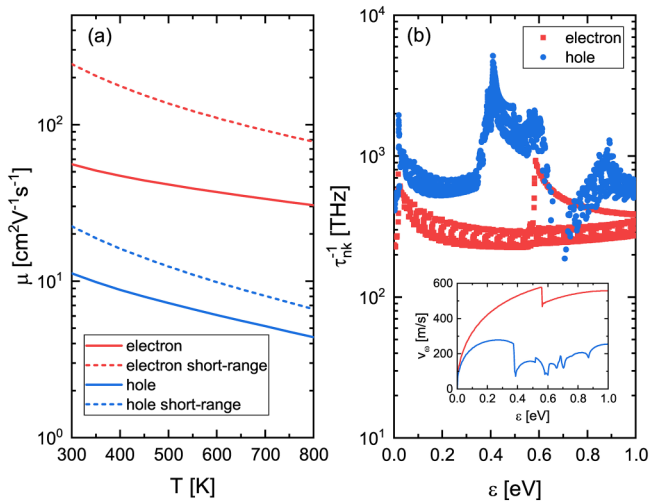

FIG. 3. (a) Intrinsic electron and hole mobilities of monolayer Tl_2O with full (solid lines) and only short-range (dashed lines) electron–phonon interactions at different temperatures. (b) Scattering rates of electrons and holes at room temperature, with the inset plotting the averaged velocity of electrons and holes as a function of energy.

The low κ_l of monolayer Tl_2O can be intuitively understood from the special phonon features. Usually, κ_l is mainly contributed by low-frequency phonons due to relatively high group velocity and relatively low scattering rates. Nevertheless, in monolayer Tl_2O, the low-frequency phonons are strongly suppressed because the effect of heavy Tl atoms completely acts on the low-frequency part, leading to low phonon group velocity that is even smaller than other low-κ_l monolayer materials with heavy atoms.[19–22] On the other hand, the phonon scattering rates of monolayer Tl_2O reach as high as 100 THz, also larger than that of many low-κ_l materials.[20,22,51] The low phonon group velocity and high phonon scattering rates jointly determine the ultralow lattice thermal conductivity. The lower limit to the κ_l of monolayer Tl_2O was calculated using the models for the amorphous phase.[64–66] A minimum thermal conductivity model proposed by Cahill *et al.*[64] was widely used. However, as some experimental thermal conductivities are found below the Cahill model,[67,68] recently, Agne *et al.*[65] developed a diffusion minimum thermal conductivity model, which usually predicts a lower thermal conductivity than that of Cahill model. More importantly, the Cahill model[64] needs the speeds of sound for acoustic phonons, which cannot be well defined for the out-of-plane acoustic (ZA) modes in 2D materials. Therefore, we employed the Ange model[65] that takes only the phonon density of states which can be directly obtained from the DFT calculations (cf. Sec. IV in the supplementary material). The calculated amorphous limit of the κ_l of monolayer Tl_2O is about 0.1 $Wm^{-1}K^{-1}$ in the temperature range of 300–800 K, as shown in Fig. 2(a).

Figure 3(a) shows the intrinsic electron and hole mobilities of monolayer Tl_2O at different temperatures, with room temperature values of 56 and 11 $cm^2 V^{-1} s^{-1}$, respectively. The hole mobility is much smaller than the electron mobility, due to the lower velocity and higher scattering rates, as shown in Fig. 3(b). The heavier hole effective mass results in the lower velocity, as well as the higher scattering rates due to large scattering channels. As temperature increases, the electron and hole mobilities reduce monotonically, by 45% and 60% at 800 K, respectively. The earlier participation of the second valley scattering, around 0.36 eV for holes compared to 0.56 eV for electrons, leads to the faster reduction of hole mobility, because the contribution from high-energy carriers is increased at elevated temperatures. The sudden decline of the hole scattering rates around 0.70 eV is due to the small density of states corresponding to few available states in the scattering processes. It is noticed that previous estimation based on the parabolic band and acoustic deformation potential model[27] overestimate the mobilities by orders of magnitude. An important reason accounting for the overestimation is the ignorance of long-range polar LO phonons scattering, which is found to play a significant role in monolayer Tl_2O. The scattering rates of electrons and holes display a large jump at a very small energy of 12 meV, corresponding to the onset of emission process of LO phonons of monolayer Tl_2O, which tallies with the common feature of strong polar materials.[32,33,40,69] If only considering the short-range phonon scattering, the obtained electron and hole mobilities are much larger, up to 243 and 22 $cm^2 V^{-1} s^{-1}$ at room temperature, about four and two times larger than their real values, respectively. The obtained results are still much smaller than the values from the semiempirical models, indicating that the full description of the band structure and electron–phonon scattering is important for electrical transport properties.

Generally, α and σ have opposite carrier concentration dependence,[30,31,51] thus, for thermoelectric materials, the electrical

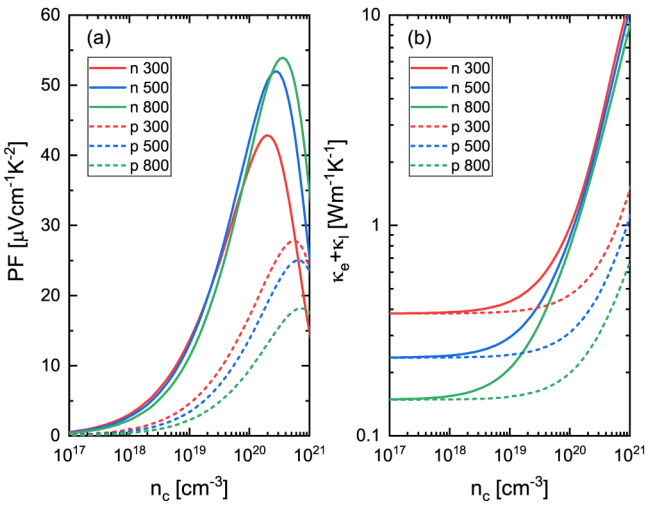

FIG. 4. Carrier concentration dependence of (a) power factor and (b) total thermal conductivity of n- and p-type monolayer Tl_2O at several temperatures.

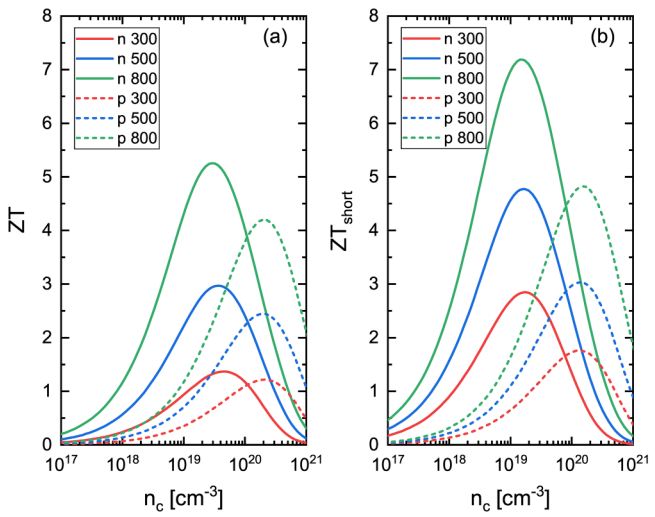

FIG. 5. Thermoelectric zT of n- and p-type monolayer Tl_2O with electrical transport properties calculated including (a) full and (b) only short-range electron–phonon scattering as a function of carrier concentration at different temperatures.

performance is integrally gauged by the PF. The PF of n- and p-type monolayer Tl_2O as a function of carrier concentration is plotted in Fig. 4(a), which shows a peak shape due to the decrease of α^2 accompanied by the increase of σ. The maximum PFs of n- and p-type systems at room temperature are 43 and $28\,\mu V\,cm^{-1}\,K^{-2}$, respectively. As temperature increases, the maximum PF of the n-type system increases, whereas it decreases for the p-type system. Figure 4(b) shows the total thermal conductivity, $\kappa = \kappa_e + \kappa_l$, at different concentrations and temperatures. Since the phonon scattering by electrons is negligible especially in low-κ_l semiconductors, it is not considered and thus κ_l is independent of carrier concentration. At low concentration, κ remains almost unchanged due to the main contribution from κ_l and negligible contribution from κ_e. As concentration increases, κ_e increases rapidly once the electron concentration exceeds $10^{18}\,cm^{-3}$ and the hole concentration exceeds $10^{19}\,cm^{-3}$. As a consequence, the optimal carrier concentration corresponding to the maximum zT shifts to a relatively smaller value as compared to that of PF, as shown in Fig. 5(a). In the temperature range of 300–800 K, the optimal concentration for maximum zT does not change much, around $4 \times 10^{19}\,cm^{-3}$ for the n-type system and about $2 \times 10^{20}\,cm^{-3}$ for the p-type system. At room temperature, corresponding to the optimal concentration, the PFs are 31 and $23\,\mu V\,cm^{-1}\,K^{-2}$ for n- and p-type systems, respectively, whereas the κ are 0.71 and $0.56\,Wm^{-1}\,K^{-1}$ in which the lattice contribution is as much as 53%–68%.

The room temperature zT of monolayer Tl_2O is larger than unity in both n- and p-type systems, as high as 1.4 and 1.2, respectively, outperforming many other 2D materials estimated by the first-principles calculations[50,51] and phenomenological models.[19–22] At 800 K, the maximum zT increase up to 5.3 and 4.2 for n- and p-type systems, respectively, about 3.5 times larger than that at room temperature. As temperature increases from 300 to 800 K, the PF corresponding to each optimal carrier concentration of zT decreases about 40% while the reduction of κ is a little larger, by about 50%. Therefore, the increase of zT mainly comes from the increase of temperature. A widely used strategy to enhance zT is nanostructuring the material, such as Si nanowire,[70] which is based on the fact that the mean free path (MFP) of phonons is generally larger than that of electrons. However, for the low-κ_l system like SnSe[41] and monolayer Tl_2O herein, nanostructuring cannot increase zT since the MFP of phonons is comparable with that of electrons. For instance, at room temperature, we found that about 99% of κ_l is contributed by phonons with MFP smaller than 3 nm, while about 99% of mobility is contributed by electrons and holes with MFP below 2.6 and 0.9 nm, respectively. Therefore, increasing the electrical transport properties of monolayer Tl_2O is a more effective choice. As aforementioned discussion, the electrical transport properties can be significantly increased if the long-range interaction is eliminated. Recently, it has reported that the long-range scattering from LO phonons can be suppressed by dielectric engineering[71] and thus enhancing the mobility of strong polar 2D materials significantly.[34] Here, we have a quick preliminary insight into estimate zT by only considering the short-range electron–phonon scattering, as shown in Fig. 5(b). It can be seen that zT indeed can be enhanced, up to 2.9 and 1.8 at 300 K, and 7.2 and 4.8 at 800 K, for n- and p-type systems, respectively. The practical situation, of course, is more complicated than present stage of materials exploration, since many extra factors are needed to be considered. Anyhow, the high intrinsic zT as well as the possibility of further enhancement predicted by the parameter-free first-principles calculations reveals the good thermoelectric promise of monolayer Tl_2O and would beckon further experiment on monolayer Tl_2O based thermoelectric materials.

IV. CONCLUSIONS

In conclusion, the thermoelectric potential of monolayer Tl_2O is investigated. The involved electrical and thermal transport properties are obtained by performing first-principles calculations and solving the parameter-free Boltzmann transport equation. The lattice thermal conductivity of monolayer Tl_2O is ultralow, only about 0.38 $Wm^{-1} K^{-1}$ at room temperature. The electron and hole mobilities of monolayer Tl_2O are also found to be small, only about 56 and 11 $cm^2 V^{-1} s^{-1}$ at room temperature, respectively, rather than previous estimated as high as thousands from the simplified phenomenological models. Despite the small mobility, the thermoelectric zT of monolayer Tl_2O is high due to the ultralow lattice thermal conductivity and considerably good power factor. The room temperature zT can exceed 1.2 for both n- and p-type systems, larger than many previous reported two-dimensional thermoelectric materials, whereas the zT values exceed 4.2 at 800 K. The long-range coupling interaction with polar longitudinal optical phonons plays a significant role in the scattering, especially for electrons. Thus, when the long-range polar scattering is suppressed, such as by dielectric engineering, zT has opportunity to be further improved. The comparable high zT for n- and p-type systems is beneficial in the thermoelectric device perspective, which desires the n- and p-type legs fabricated by the same parent compound. Therefore, monolayer Tl_2O possesses great promise for the thermoelectric application in a wide temperature range with high performance. These results are expected to impel the experimental studies on the monolayer Tl_2O based thermoelectric materials.

SUPPLEMENTARY MATERIAL

See the supplementary material for the convergence check of lattice thermal conductivity and carrier mobility, the GW correction of the band structure and the corresponding effect on thermoelectric zT, and the Agne model for the amorphous limit of lattice thermal conductivity.

ACKNOWLEDGMENTS

J.M. acknowledges support from the National Natural Science Foundation of China (NNSFC, No. 11804229). D.X. acknowledges support from the National Natural Science Foundation of China (NNSFC, No. 51806072). X.L. acknowledges support from the Ministry of Science and Technology of the People's Republic of China (No. 2017YFE0100600).

DATA AVAILABILITY

The data that support the findings of this study are available from the corresponding author upon reasonable request.

REFERENCES

[1]J. He and T. M. Tritt, Science **357**, eaak9997 (2017).
[2]G. J. Snyder and E. S. Toberer, Nat. Mater. **7**, 105 (2008).
[3]T. Zhu, Y. Liu, C. Fu, J. P. Heremans, J. G. Snyder, and X. Zhao, Adv. Mater. **29**, 1605884 (2017).
[4]L.-D. Zhao, S.-H. Lo, Y. Zhang, H. Sun, G. Tan, C. Uher, C. Wolverton, V. P. Dravid, and M. G. Kanatzidis, Nature **508**, 373 (2014).
[5]C. Chang, M. Wu, D. He, Y. Pei, C.-F. Wu, X. Wu, H. Yu, F. Zhu, K. Wang, Y. Chen, L. Huang, J.-F. Li, J. He, and L.-D. Zhao, Science **360**, 778 (2018).
[6]P. Ying, X. Liu, C. Fu, X. Yue, H. Xie, X. Zhao, W. Zhang, and T. Zhu, Chem. Mater. **27**, 909 (2015).
[7]L.-D. Zhao, J. He, D. Berardan, Y. Lin, J.-F. Li, C.-W. Nan, and N. Dragoe, Energy Environ. Sci. **7**, 2900 (2014).
[8]H. Liu, X. Yuan, P. Lu, X. Shi, F. Xu, Y. He, Y. Tang, S. Bai, W. Zhang, L. Chen, Y. Lin, L. Shi, H. Lin, X. Gao, X. Zhang, H. Chi, and C. Uher, Adv. Mater. **25**, 6607 (2013).
[9]D. M. Rowe, V. L. Kuznetsov, L. A. Kuznetsova, and G. Min, J. Phys. D Appl. Phys. **35**, 2183 (2002).
[10]W.-D. Liu, L. Yang, Z.-G. Chen, and J. Zou, Adv. Mater. **32**, 1905703 (2020).
[11]Q. H. Wang, K. Kalantar-Zadeh, A. Kis, J. N. Coleman, and M. S. Strano, Nat. Nanotechnol. **7**, 699 (2012).
[12]W. Choi, N. Choudhary, G. H. Han, J. Park, D. Akinwande, and Y. H. Lee, Mater. Today **20**, 116 (2017).
[13]H. Kim, B. Anasori, Y. Gogotsi, and H. N. Alshareef, Chem. Mater. **29**, 6472 (2017).
[14]D. Li, Y. Gong, Y. Chen, J. Lin, Q. Khan, Y. Zhang, Y. Li, H. Zhang, and H. Xie, Nano Micro Lett. **12**, 36 (2020).
[15]J. Wu, Y. Chen, J. Wu, and K. Hippalgaonkar, Adv. Electron. Mater. **4**, 1800248 (2018).
[16]M. Yoshida, T. Iizuka, Y. Saito, M. Onga, R. Suzuki, Y. Zhang, Y. Iwasa, and S. Shimizu, Nano Lett. **16**, 2061 (2016).
[17]K. Hippalgaonkar, Y. Wang, Y. Ye, D. Y. Qiu, H. Zhu, Y. Wang, J. Moore, S. G. Louie, and X. Zhang, Phys. Rev. B **95**, 115407 (2017).
[18]Y. Cheng, J. Yang, Q. Jiang, D. He, J. He, Y. Luo, D. Zhang, Z. Zhou, Y. Ren, and J. Xin, J. Mater. Chem. A **5**, 5163 (2017).
[19]B. Marfoua and J. Hong, ACS Appl. Mater. Interfaces **11**, 38819 (2019).
[20]Z. Rashid, A. S. Nissimagoudar, and W. Li, Phys. Chem. Chem. Phys. **21**, 5679 (2019).
[21]S. S. Naghavi, J. He, Y. Xia, and C. Wolverton, Chem. Mater. **30**, 5639 (2018).
[22]X. Zhang, C. Liu, Y. Tao, Y. Li, Y. Guo, Y. Chen, X. C. Zeng, and J. Wang, Adv. Funct. Mater. **30**, 2001200 (2020).
[23]Z. Gao and J.-S. Wang, ACS Appl. Mater. Interfaces **12**, 14298 (2020).
[24]W. Li, J. Carrete, N. A. Katcho, and N. Mingo, Comput. Phys. Commun. **185**, 1747 (2014).
[25]A. Togo, L. Chaput, and I. Tanaka, Phys. Rev. B **91**, 094306 (2015).
[26]N. Mounet, M. Gibertini, P. Schwaller, D. Campi, A. Merkys, A. Marrazzo, T. Sohier, I. E. Castelli, A. Cepellotti, G. Pizzi, and N. Marzari, Nat. Nanotechnol. **13**, 246 (2018).
[27]Y. Ma, A. Kuc, and T. Heine, J. Am. Chem. Soc. **139**, 11694 (2017).
[28]M. Sajjad, N. Singh, S. Sattar, S. De Wolf, and U. Schwingenschlögl, ACS Appl. Energy Mater. **2**, 3004 (2019).
[29]H. Wang, Y. Zhou, Z.-Y. Zeng, Y. Cheng, and Q.-F. Chen, Solid State Commun. **293**, 40 (2019).
[30]H. H. Huang, G. Xing, X. Fan, D. J. Singh, and W. T. Zheng, J. Mater. Chem. C **7**, 5094 (2019).
[31]C. Wang, S. Wei, and G. Gao, ACS Appl. Nano Mater. **2**, 4061 (2019).
[32]T.-H. Liu, J. Zhou, B. Liao, D. J. Singh, and G. Chen, Phys. Rev. B **95**, 075206 (2017).
[33]J. Ma, A. S. Nissimagoudar, and W. Li, Phys. Rev. B **97**, 045201 (2018).
[34]J. Ma, D. Xu, R. Hu, and X. Luo, J. Appl. Phys. **128**, 035107 (2020).
[35]D. A. Broido, M. Malorny, G. Birner, N. Mingo, and D. A. Stewart, Appl. Phys. Lett. **91**, 231922 (2007).
[36]B. Qiu, Z. Tian, A. Vallabhaneni, B. Liao, J. M. Mendoza, O. D. Restrepo, X. Ruan, and G. Chen, Europhys. Lett. **109**, 57006 (2015).
[37]S. Poncé, W. Li, S. Reichardt, and F. Giustino, Rep. Prog. Phys. **83**, 036501 (2020).
[38]F. Giustino, Rev. Mod. Phys. **89**, 015003 (2017).
[39]M. Fiorentini and N. Bonini, Phys. Rev. B **94**, 085204 (2016).
[40]J.-J. Zhou and M. Bernardi, Phys. Rev. B **94**, 201201(R) (2016).
[41]J. Ma, Y. Chen, and W. Li, Phys. Rev. B **97**, 205207 (2018).

[42]S. Poncé, E. R. Margine, and F. Giustino, Phys. Rev. B **97**, 121201(R) (2018).
[43]F. Meng, J. Ma, J. He, and W. Li, Phys. Rev. B **99**, 045201 (2019).
[44]S. Poncé, D. Jena, and F. Giustino, Phys. Rev. B **100**, 085204 (2019).
[45]S. Li, Z. Tong, and H. Bao, J. Appl. Phys. **126**, 025111 (2019).
[46]F. Meng, S. Sun, J. Ma, C. Chronister, J. He, and W. Li, Mater. Today Phys. **13**, 100217 (2020).
[47]J. Park, Y. Xia, and V. Ozoliņš, Phys. Rev. Appl. **11**, 014058 (2019).
[48]J. Park, Y. Xia, A. M. Ganose, A. Jain, and V. Ozoliņš, Phys. Rev. Appl. **14**, 024064 (2020).
[49]J. Ma, A. S. Nissimagoudar, S. Wang, and W. Li, Phys. Status Solidi RRL **14**, 2000084 (2020).
[50]T. Deng, X. Yong, W. Shi, C. K. Gan, W. Li, K. Hippalgaonkar, J.-C. Zheng, X. Wang, S.-W. Yang, J.-S. Wang, and G. Wu, Adv. Electron. Mater. **5**, 1800892 (2019).
[51]J. Ma, F. Meng, J. He, Y. Jia, and W. Li, ACS Appl. Mater. Interfaces **12**, 43901 (2020).
[52]W. Li, Phys. Rev. B **92**, 075405 (2015).
[53]P. Giannozzi, O. Andreussi, T. Brumme *et al.*, J. Phys. Condens. Matter **29**, 465901 (2017).
[54]M. van Setten, M. Giantomassi, E. Bousquet, M. Verstraete, D. Hamann, X. Gonze, and G.-M. Rignanese, Comput. Phys. Commun. **226**, 39 (2018).
[55]J. P. Perdew, K. Burke, and M. Ernzerhof, Phys. Rev. Lett. **77**, 3865 (1996).
[56]H. Sabrowsky, Z. Anorg. Allg. Chem. **381**, 266 (1971).
[57]S. Poncé, E. Margine, C. Verdi, and F. Giustino, Comput. Phys. Commun. **209**, 116 (2016).
[58]T. Sohier, M. Gibertini, M. Calandra, F. Mauri, and N. Marzari, Nano Lett. **17**, 3758 (2017).
[59]T. Sohier, M. Calandra, and F. Mauri, Phys. Rev. B **94**, 085415 (2016).
[60]A. Marini, C. Hogan, M. Gruning, and D. Varsano, Comput. Phys. Commun. **180**, 1392 (2009).
[61]T. M. Tritt and M. A. Subramanian, MRS Bull. **31**, 188 (2006).
[62]C. Ataca, H. Şahin, and S. Ciraci, J. Phys. Chem. C **116**, 8983 (2012).
[63]J. Ma, W. Li, and X. Luo, Appl. Phys. Lett. **105**, 082103 (2014).
[64]D. G. Cahill, S. K. Watson, and R. O. Pohl, Phys. Rev. B **46**, 6131 (1992).
[65]M. T. Agne, R. Hanus, and G. J. Snyder, Energy Environ. Sci. **11**, 609 (2018).
[66]W.-X. Zhou, Y. Cheng, K.-Q. Chen, G. Xie, T. Wang, and G. Zhang, Adv. Funct. Mater. **30**, 1903829 (2020).
[67]Z. Cheng, A. Weidenbach, T. Feng, M. B. Tellekamp, S. Howard, M. J. Wahila, B. Zivasatienraj, B. Foley, S. T. Pantelides, L. F. J. Piper, W. Doolittle, and S. Graham, Phys. Rev. Mater. **3**, 025002 (2019).
[68]L. Wang, M. Hong, Q. Sun, Y. Wang, L. Yue, S. Zheng, J. Zou, and Z.-G. Chen, ACS Appl. Mater. Interfaces **12**, 36370 (2020).
[69]W. Li, S. Poncé, and F. Giustino, Nano Lett. **19**, 1774 (2019).
[70]A. I. Hochbaum, R. Chen, R. D. Delgado, W. Liang, E. C. Garnett, M. Najarian, A. Majumdar, and P. Yang, Nature **451**, 163 (2008).
[71]D. Jena and A. Konar, Phys. Rev. Lett. **98**, 136805 (2007).